Electronic Supplementary Material (ESI) for Journal of Materials Chemistry A.

Helical PdPtAu Nanowires Bounded with High-Index Facets Selectively Switch the Pathway of Ethanol Electrooxidation

Jing-Xiao Tang,[a] Na Tian,[a,*] Liang-Ping Xiao,[a] Qing-Song Chen,[b] Qiong Wang,[a] Zhi-You Zhou[a] and Shi-Gang Sun[a,*]

[a]State Key Laboratory of Physical Chemistry of Solid Surfaces, Collaborative Innovation Center of Chemistry for Energy Materials, College of Chemistry and Chemical Engineering, Xiamen University, Xiamen 361005, China.

[b]State Key Laboratory of Structural Chemistry, Fujian Institute of Research on the Structure of Matter, Chinese Academy of Sciences, Fuzhou, Fujian 350002, China

Corresponding Authors. E-mail: tnsd@xmu.edu.cn (Na Tian); sgsun@xmu.edu.cn (Shi-Gang Sun)

Chemicals

Glassy-carbon electrode (φ = 3 mm) was purchased from Takai Carbon Co., LTD (Tokyo, Japan). Commercial Pt black was purchased from Alfa Aesar (Tianjin, China). Commercial Pd black and Nafion were acquired from Sigma Aldrich. NaOH, ethanol, $PdCl_2$, $H_2PtCl_6 \cdot 6H_2O$ and $HAuCl_4 \cdot 4H_2O$ were purchased from Sinopharm Chemical Reagent Co., LTD. (Shanghai, China). Perchloric acid (EMSURE® ACS) was purchased from Merck. Argon (99.99%) and CO (99.9%) were purchased from Linde gas Co., LTD (Xiamen). All the chemicals were used as received without further purification. The ultra-pure water (18 MΩ cm) for cleaning glassware and solution preparation was produced from the Millipore system.

Materials characterization

The morphologies of NWs were conducted with a scanning electron microscope (SEM) on Hitachi S-4800 and transmission electron microscope (TEM) on JEM 2100 and FEI F20 at 200 kV. The composition of NWs was obtained by SEM-energy dispersive X-ray spectroscopy (SEM-EDS, Hitachi S-4800) and X-ray photoelectron spectroscopy (XPS, ESCALAB 250 Xi). The XPS spectra were all corrected by C 1*s* peak (284.8 eV).

Electrocatalytic measurements

All electrochemical measurements were carried out on a CHI 760E electrochemical workstation (Shanghai Chenhua Co., China). Electrochemical measurements were conducted in a standard three electrode cell. The glassy-carbon electrode coated with catalyst was used as the working electrode. A platinum foil and saturated calomel electrode (SCE) served as the counter electrode and reference electrode, respectively. All solutions were deaerated by purging with high purity Ar for 10 min before measurements. Electrocatalytic oxidation of ethanol was carried out in 0.1 M ethanol + 0.1 M NaOH at room temperature. The cyclic voltammograms (CVs) was

recorded between –0.85 and 0.10 V at a sweep rate of 50 mV s^{-1} to evaluate the catalytic activity of the catalysts. The stability of the catalysts was evaluated by the *i–t* curve recorded at –0.30 V.

Electrochemical in situ FTIR studies for CO adsorption and ethanol oxidation

Electrochemical in situ FTIR reflection spectroscopic experiments were carried out on a Nicolet 8700 FTIR spectrometer (Thermo Scientific) equipped with a liquid nitrogen-cooled MCT-A detector and an EverGlo IR source for study the product selectivity of ethanol electrooxidation on different catalysts. The experimental details of in situ FTIR experiments are the same as those reported in our previous work.[1] The resulting spectra were reported as the relative change in reflectivity:

$$\frac{\Delta R}{R} = \frac{R(E_S) - R(E_R)}{R(E_R)} \quad (1)$$

The $R(E_S)$ and $R(E_R)$ are the single-beam spectra collected at sample potential (E_S) and reference potential (E_R), respectively. For CO adsorption, the E_S varied from –0.90 V to –0.70 V with the spectral resolution being 8 cm^{-1}, the E_R was fixed at 0 V after CO oxidation. The potential step is 50 mV. For ethanol oxidation, the E_R was fixed at –0.80 V prior to ethanol oxidation. The E_S varied from –0.70 V to 0.10 V with the spectral resolution being 8 cm^{-1} and the potential step being 100 mV.

Estimation of mass activity

It is hard to measure accurately the mass of the Pd-based nanowires deposited on the glassy carbon electrode, since the deposited metal cannot be fully removed from the electrode surface by ultrasound. Alternatively, we estimated the mass activity (j_m) from the surface area specific activity (j_S) according to the ratio of area to volume for smooth nanowires, as indicated in *E*q(2) and (3).

$$S/V = \frac{2\pi rl}{\pi r^2 l} = \frac{2}{r} \qquad (2)$$

$$\frac{j_S}{j_m} = \frac{\frac{i}{S}}{\frac{i}{m}} = \frac{m}{S} = \frac{V\rho}{S} = \frac{r\rho}{2} \qquad (3)$$

Where r is the radius, l is the length, and ρ is the density of the nanowire.

The average diameters of the $Pd_{14}Pt_5$ and $Pd_{14}Pt_5Au_2$ NWs are 37.3 ± 2.9 and 35.5 ± 3.2 nm, respectively. The mean density (ρ) of $Pd_{14}Pt_5$ and $Pd_{14}Pt_5Au_2$ are about 14.5 and 15.0 g cm^{-3}, respectively. According to the specific activities of $Pd_{14}Pt_5$ NWs (3.1 mA cm^{-2}) and $Pd_{14}Pt_5Au_2$ NWs (4.4 mA cm^{-2}) for ethanol oxidation, the mass activities are estimated to be 230 and 330 A per gram of noble metal (Pd + Pt + Au), respectively. Considering the coarse surface of $Pd_{14}Pt_5$ NWs and $Pd_{14}Pt_5Au_2$ NWs, which will result in the underestimation of specific surface area (S/m), the mass activities will be larger than the above estimated values.

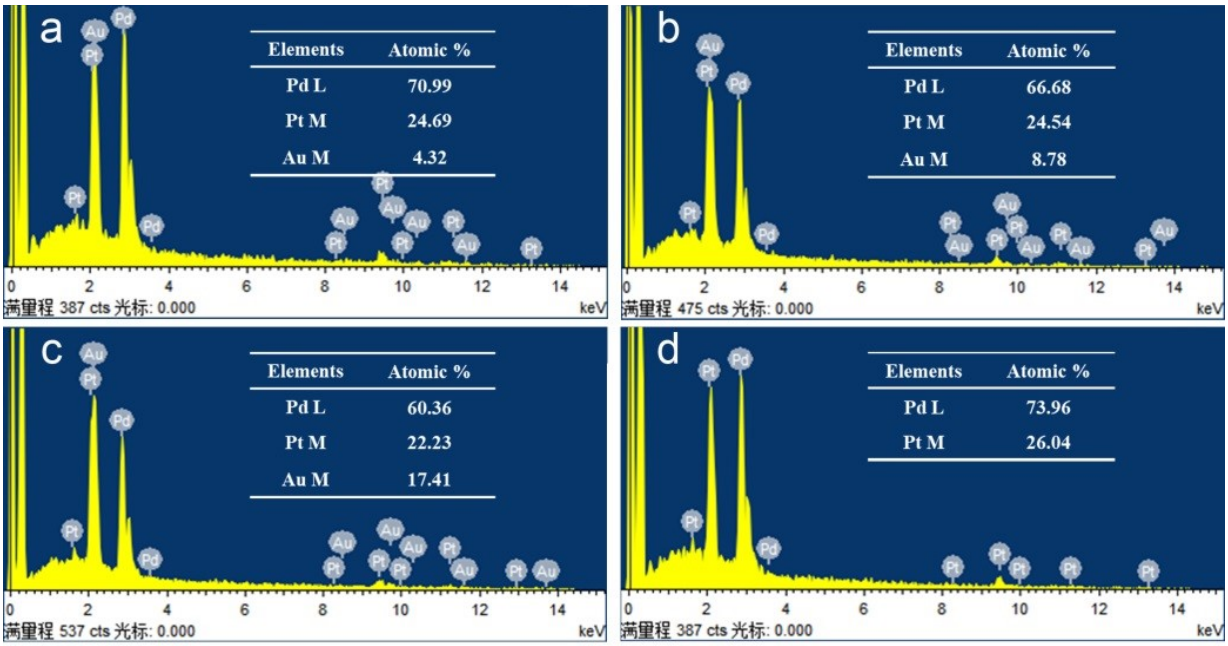

Fig. S1 SEM-EDS of (a) $Pd_{14}Pt_5Au_1$ NWs, (b) $Pd_{14}Pt_5Au_2$ NWs, (c) $Pd_{14}Pt_5Au_4$ NWs, (d) $Pd_{14}Pt_5$ NWs.

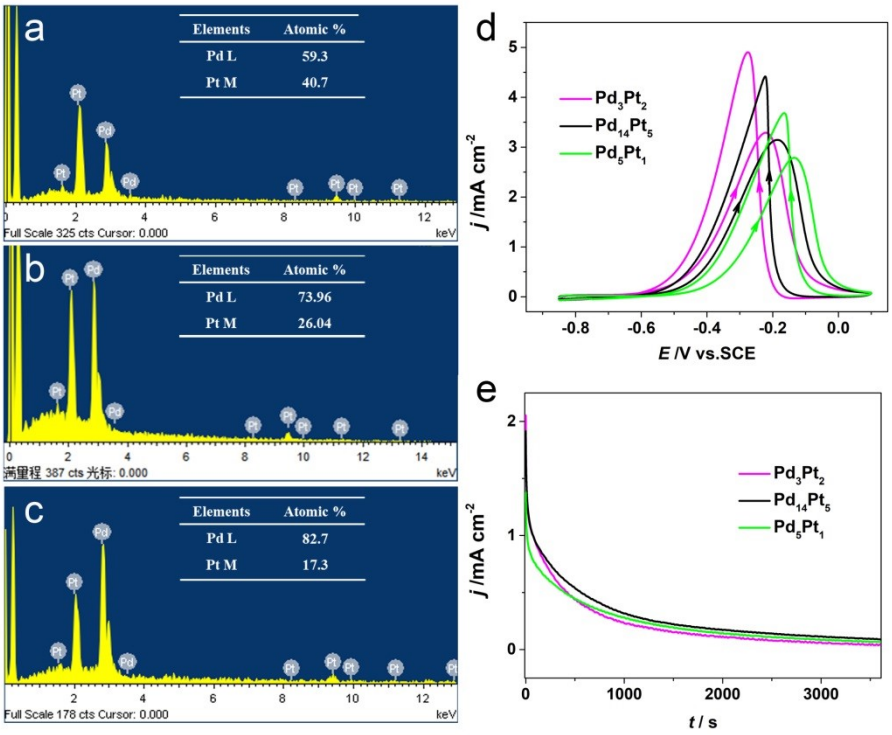

Fig. S2 SEM-EDS of (a) Pd_3Pt_2 NWs, (b) $Pd_{14}Pt_5$ NWs, (c) Pd_5Pt_1 NWs. (d) CVs and (e) *i*–*t* curves of ethanol oxidation on PdPt NWs in Ar-saturated 0.1 M ethanol + 0.1 M NaOH solution.

We have optimized the ratio of Pd and Pt in nanowires before Au doping. As shown in Fig. S2, three PdPt NWs with the molar ratio of Pd : Pt of 59.3 : 40.7, 74.0 : 26.0, and 82.7 :17.3 were prepared. These ratios are close to 3 : 2, 14 : 5, and 5 : 1, and thus the samples are denoted as Pd_3Pt_2, $Pd_{14}Pt_5$, and Pd_5Pt_1 NWs, respectively. The positive-going peak current density in CV curves of ethanol oxidation on Pd_3Pt_2 NWs, $Pd_{14}Pt_5$, and Pd_5Pt_1 NWs is 3.3, 3.1, and 2.8 mA cm^{-2}, respectively. The steady-state current density at –0.30 V of Pd_3Pt_2, $Pd_{14}Pt_5$, and Pd_5Pt_1 NWs are 0.04, 0.09, and 0.07 mA cm^{-2}, respectively. Clearly, $Pd_{14}Pt_5$ NWs show the highest stability and moderate catalytic activity, thus we choose the Pd/Pt ratio of 14 : 5 for further tuning the Au content.

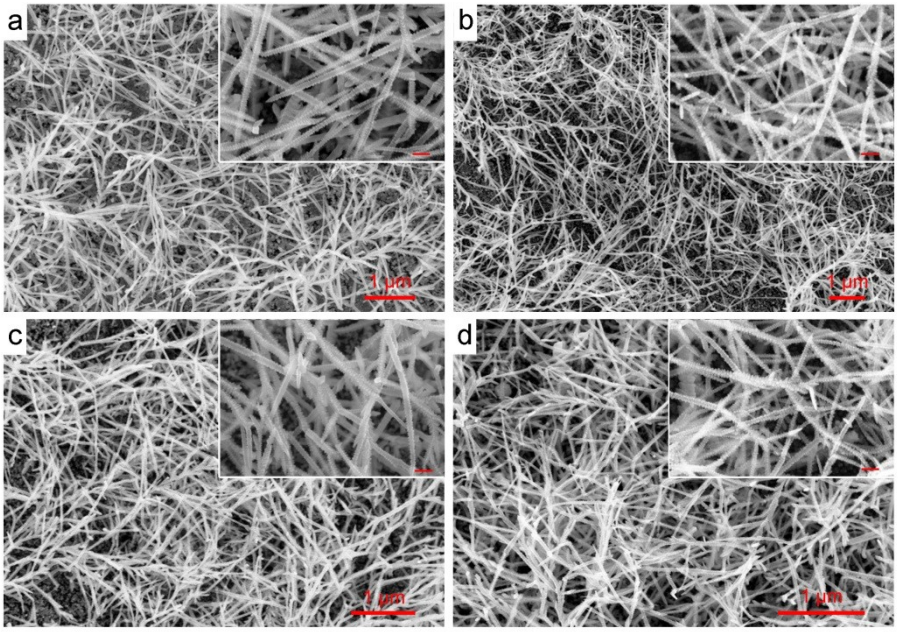

Fig. S3 SEM images of (a) $Pd_{14}Pt_5$ NWs, (b) $Pd_{14}Pt_5Au_1$ NWs, (c) $Pd_{14}Pt_5Au_2$ NWs, (d) $Pd_{14}Pt_5Au_4$ NWs. The insets are the corresponding high-magnification SEM images and all scale bars in the insets are 100 nm.

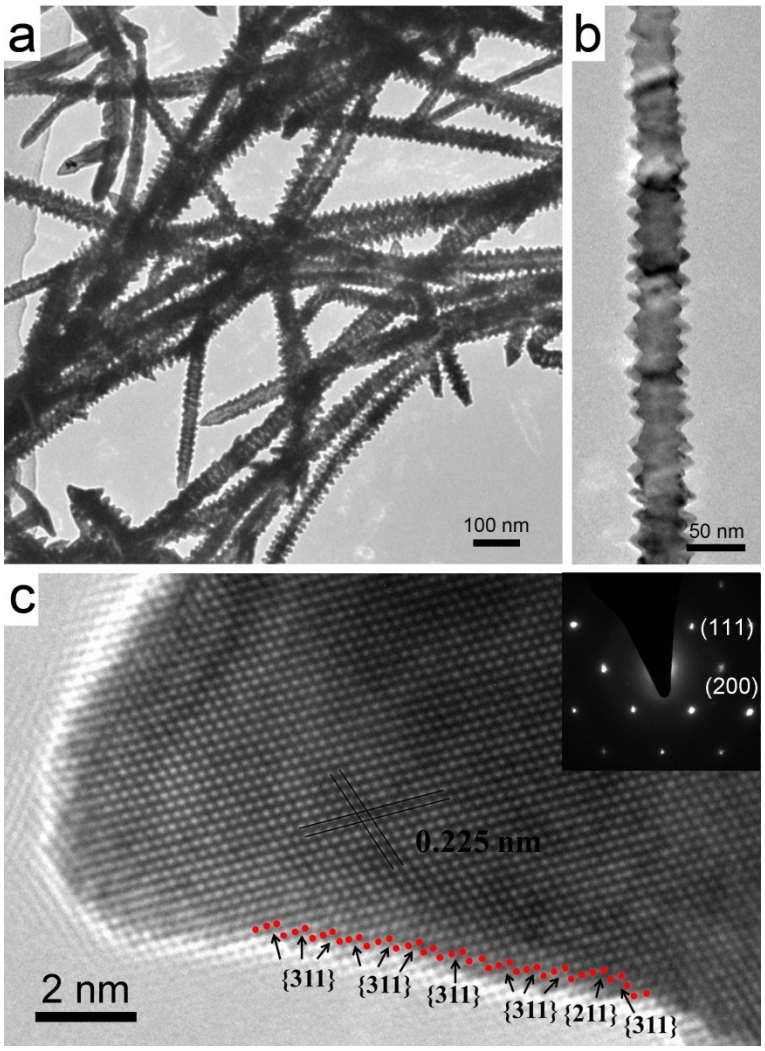

Fig. S4 (a, b) TEM images of $Pd_{14}Pt_5$ NWs. (c) HRTEM image and selected area electron diffraction of $Pd_{14}Pt_5$ NWs along [0 -1 1] crystal axis.

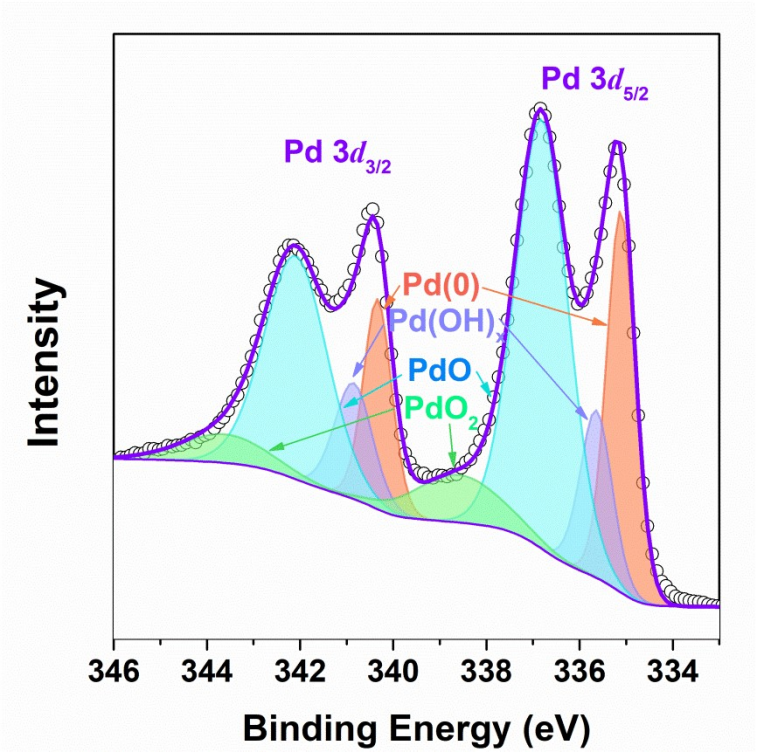

Fig. S5 Peak fitting of the XPS spectrum of Pd black.

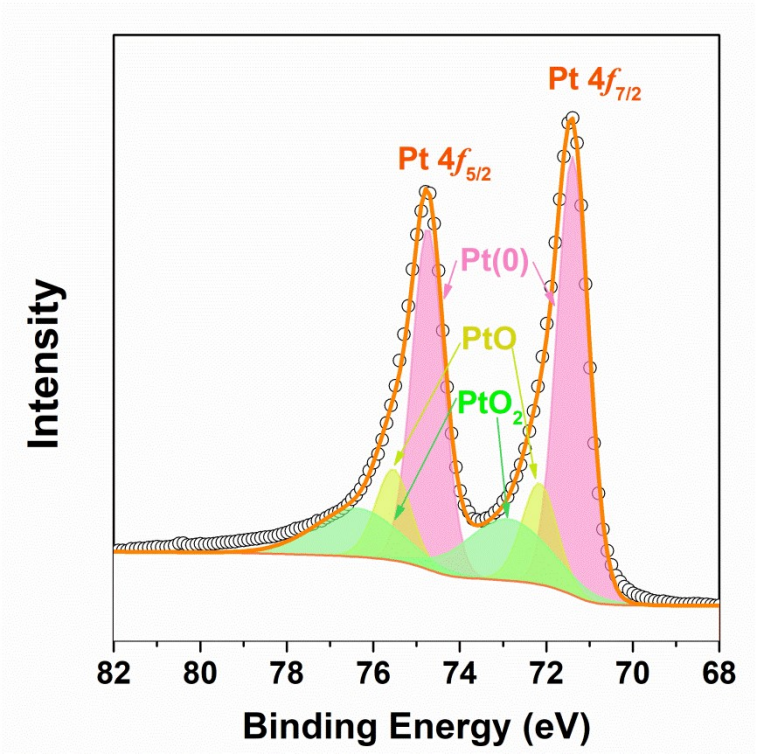

Fig. S6 Peak fitting of the XPS spectrum of Pt black.

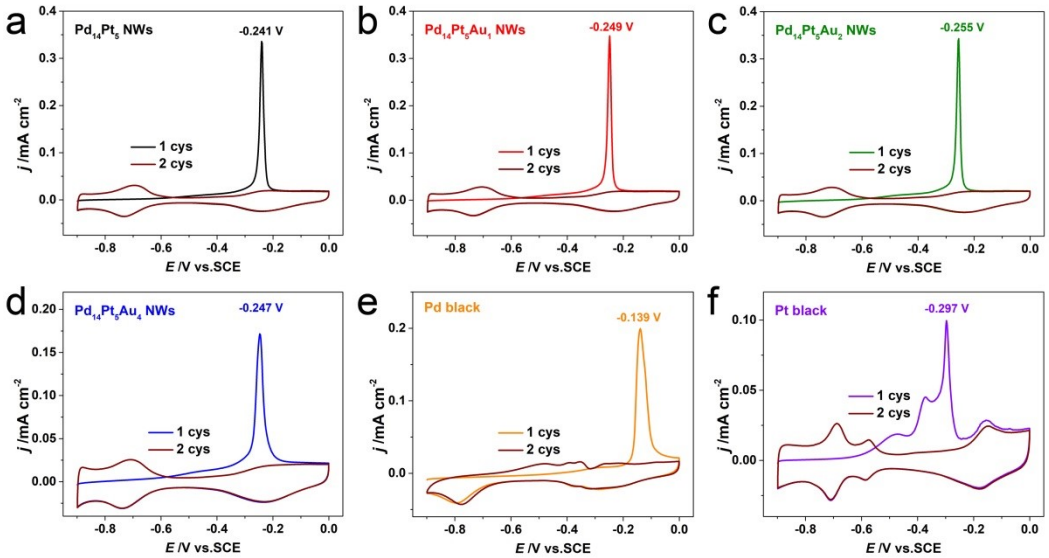

Fig. S7 CVs of CO stripping on (a) $Pd_{14}Pt_5$ NWs, (b) $Pd_{14}Pt_5Au_1$ NWs, (c) $Pd_{14}Pt_5Au_2$ NWs, (d) $Pd_{14}Pt_5Au_4$ NWs, (e) Pd black, and (f) Pt black in 0.1 M NaOH solution.

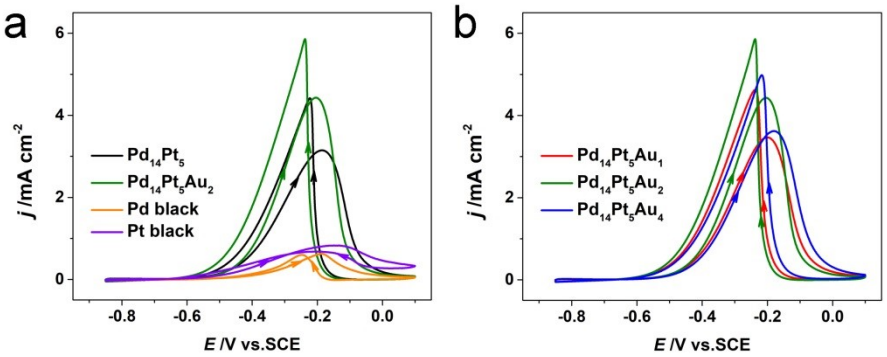

Fig. S8 CVs of ethanol oxidation on PdPtAu NWs, PdPt NWs, Pd black, and Pt black in Ar-saturated 0.1 M ethanol + 0.1 M NaOH solution.

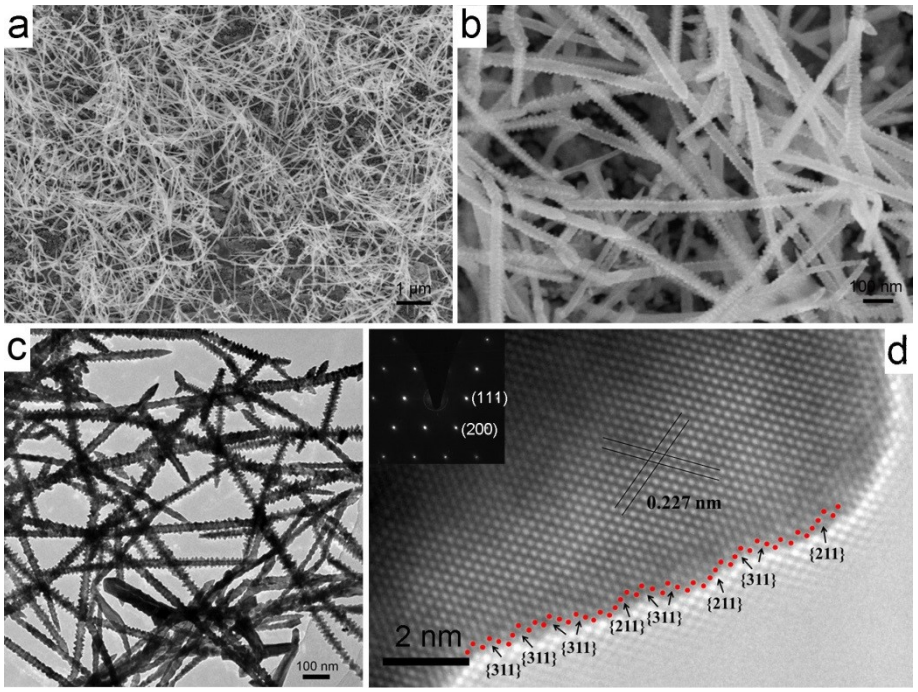

Fig. S9 Representative SEM and TEM images of $Pd_{14}Pt_5Au_2$ NWs after the stability test of ethanol electrooxidation. (a) low- and (b) high-magnification SEM images. (c) TEM image. (d) HRTEM image and the selected area electron diffraction (inset) along [0 -1 1] crystal axis. Note that the observed direction of [0 -1 1] axis is not the same as that in Fig. 1f ([001] axis), so that {*hk*0} sites could not be observed in (d).

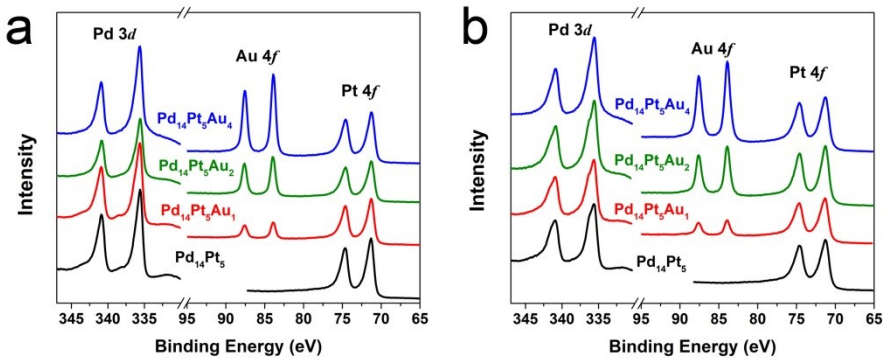

Fig. S10 Pd 3*d*, Pt 4*f* and Au 4*f* XPS spectra of NWs (a) before and (b) after the stability test of ethanol electrooxidation.

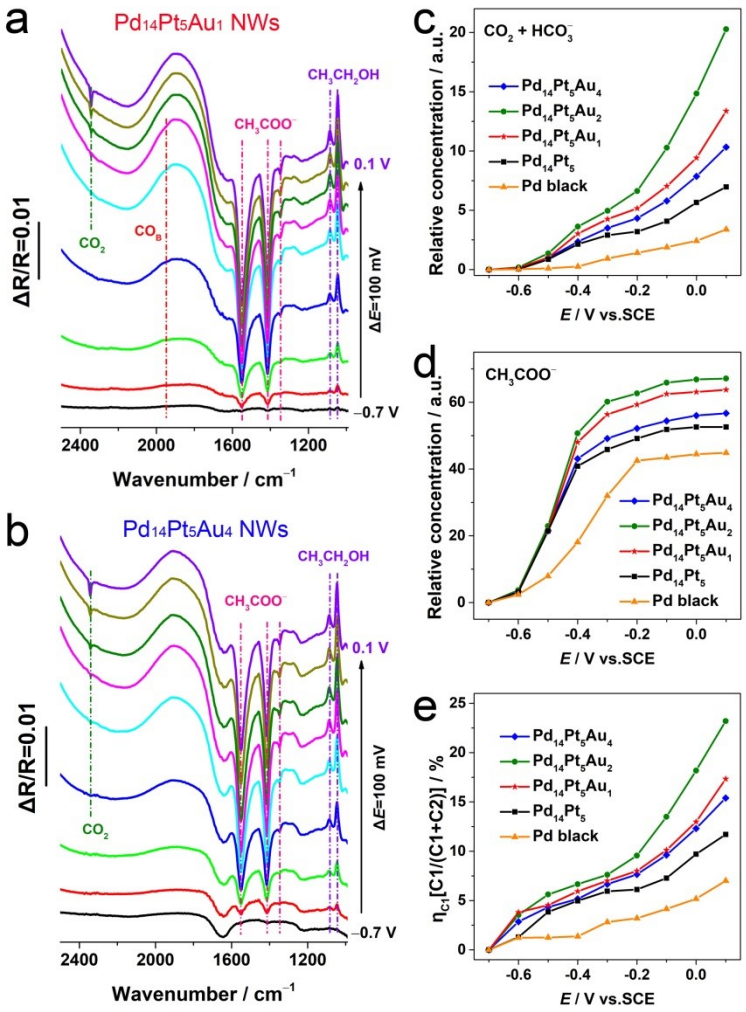

Fig. S11 In situ FTIR spectra of ethanol oxidation in 0.1 M ethanol + 0.1 M NaOH solution on (a) $Pd_{14}Pt_5Au_1$ NWs and (b) $Pd_{14}Pt_5Au_4$ NWs. The relative concentration of (d) CO_2 + HCO_3^-, and (e) CH_3COO^-. (f) The selectivity of C1 products on different catalysts.

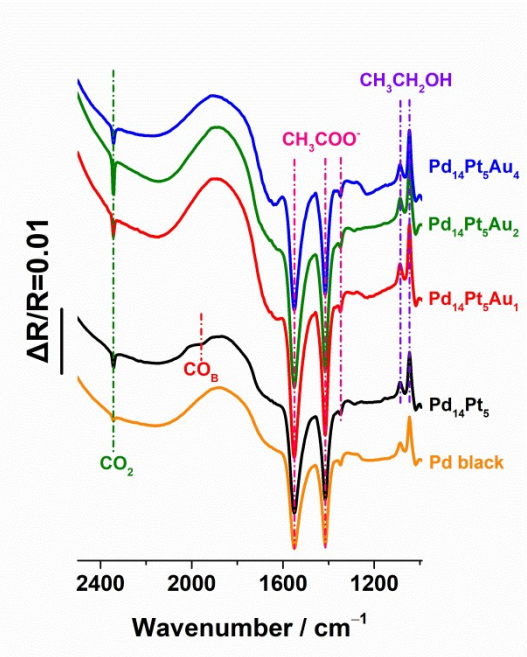

Fig. S12 In situ FTIR spectra of ethanol oxidation on different catalysts at 0.10 V in 0.1 M ethanol + 0.1 M NaOH solution.

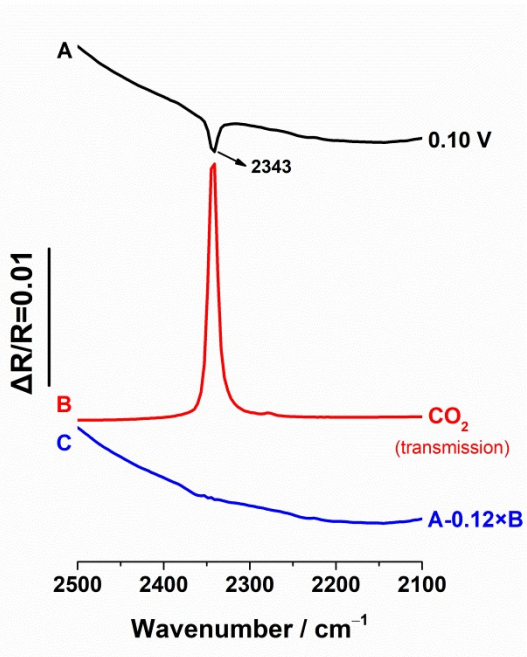

Fig. S13 Quantification of CO_2 as product of ethanol oxidation on $Pd_{14}Pt_5$ NWs. In situ FTIR spectrum of ethanol oxidation at 0.10 V (A). Transmission IR spectrum of saturated CO_2 (B). The resulting spectrum of A – 0.1243 × B (C).

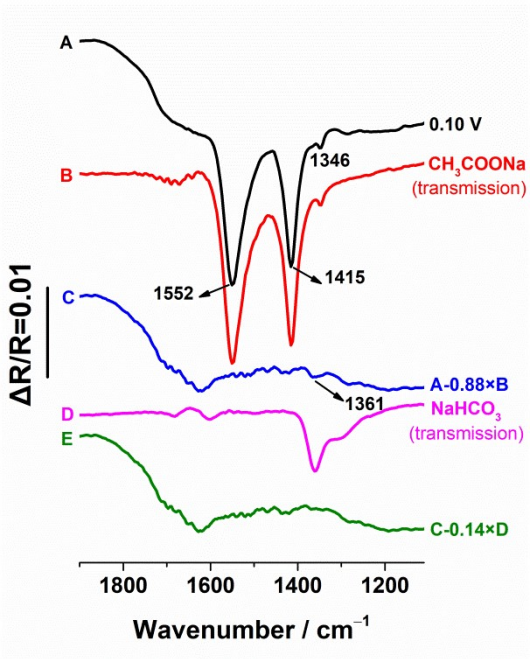

Fig. S14 Quantification of acetate and carbonate as products of ethanol oxidation on $Pd_{14}Pt_5$ NWs. In situ FTIR spectrum of ethanol oxidation at 0.10 V (A). Transmission IR spectrum of 60 mM CH_3COONa (B). The resulting spectrum of A – 0.8764 × B (C). Transmission IR spectrum of 20 mM $NaHCO_3$ (D). The resulting spectrum of C – 0.1370 × D (E).

The reaction process and products involved in the ethanol oxidation process are as follows:

$$CH_3CH_2OH + 5OH^- \rightarrow CH_3COO^- + 4H_2O + 4e^- \quad (4)$$

$$CH_3CH_2OH + 12OH^- \rightarrow 2CO_2 + 9\ H_2O + 12\ e^- \quad (5)$$

$$CO_2 + 2OH^- \rightarrow CO_3^{2-} \quad (6)$$

$$CO_3^{2-} + CO_2 \rightarrow 2HCO_3^- \quad (7)$$

In this study, all the CO_3^{2-} was converted to HCO_3^- because CO_2 was excessive. Therefore, the products of ethanol oxidation include CO_2, HCO_3^- and CH_3COO^-. CO_2 and HCO_3^- are complete oxidation species, named C1 products. CH_3COO^- is incomplete oxidation species, named C2 product. Taking $Pd_{14}Pt_5$ NWs as an example (Fig. S13), the calculation process of CO_2 relative

concentration is as follows: spectrum A is in situ FTIR spectrum of ethanol oxidation at 0.10 V, spectrum B is transmission IR spectrum of saturated CO_2. Through subtracting spectrum method, spectrum C (A − 0.1243 × B) is obtained, in which the characteristic absorption of CO_2 disappears. Same as the CO_2, the relative concentration of CH_3COO^- and HCO_3^- can be obtained, as shown in Figure S14.

Table S1 Atomic ratio of Pd, Pt, and Au acquired from SEM-EDS and XPS analysis of the nanowires.

Catalysts	Pd : Pt : Au from EDS	Pd : Pt : Au from XPS
$Pd_{14}Pt_5$	74.0 : 26.0 : 0	57.8 : 42.2 : 0
$Pd_{14}Pt_5Au_1$	71.0 : 24.7 : 4.3	56.6 : 37.3 : 6.1
$Pd_{14}Pt_5Au_2$	66.7 : 24.5 : 8.8	54.3 : 34.3 : 11.4
$Pd_{14}Pt_5Au_4$	60.4 : 22.2 : 17.4	47.0 : 29.0 : 24.0

Table S2 Binding energy (BE) and relative intensity obtained from the Pd 3*d*, Pt 4*f* and Au 4*f* XPS spectra of $Pd_{14}Pt_5Au_2$ NWs.

Species	BE (eV)	Relative Intensity (%)	Species	BE (eV)	Relative Intensity (%)	Species	BE (eV)	Relative Intensity (%)
Pd(0)	335.50	47.8	Pt(0)	71.20	49.1	Au(0)	83.91	85.1
$Pd(OH)_x$	336.00	20.2	PtO	71.80	40.5	Au(I)	84.61	14.9
PdO	336.40	16.7	PtO_2	73.30	10.4	/	/	/
PdO_2	337.10	15.3	/	/	/	/	/	/

Table S3 Binding energy (BE) and relative intensity obtained from the Pd 3*d* XPS spectra of commercial Pd black and the Pt 4*f* XPS spectra of commercial Pt black.

Species	BE (eV)	Relative Intensity (%)	Species	BE (eV)	Relative Intensity (%)
Pd(0)	335.14	25.3	Pt(0)	71.39	61.2
$Pd(OH)_x$	335.64	12.3	PtO	72.19	15.9
PdO	336.84	52.7	PtO_2	72.89	22.9
PdO_2	338.64	9.7	/	/	/

Table S4 Comparison of catalytic activities of various catalysts for ethanol electrooxidation.

Catalysts	Electrolyte	Scan rate/mV s^{-1}	j_f/mA cm^{-2}	Refs.
$Pd_{14}Pt_5Au_2$ nanowires	**0.1 M ethanol + 0.1 M NaOH**	**50**	**4.4**	**This work**
Pd tetrahexahedra	0.1 M ethanol + 0.1 M NaOH	10	1.84	Ref. 2
Pd nanorods	0.1 M ethanol + 0.1 M NaOH	10	1.3	Ref. 3
Au@Pd_1-Pt_1 H-Ss	1.0 M ethanol + 1.0 M KOH	50	3.66	Ref. 4
Pd/$Ni(OH)_2$/rGO	1.0 M ethanol + 1.0 M KOH	50	3.72	Ref. 5
2D PdAg nanodendrites	1.0 M ethanol + 1.0 M KOH	50	3.74	Ref. 6
Pd/ATNBP-30%	1 M ethanol + 1 M NaOH	50	1.09	Ref. 7
10% PdAu nanowires	0.5 M ethanol + 0.5 M KOH	50	2.56	Ref. 8
PdAuCu nanoparticles	1.0 M ethanol + 1.0 M KOH	50	3.55	Ref. 9
Pd/$NiMoO_4$-C	1.0 M ethanol + 1.0 M KOH	50	1.9	Ref. 10
Pd/AG-BP	1 M ethanol + 1 M NaOH	50	2.17	Ref. 11
Pd-Pt-Ag nanosheets	0.5 M ethanol + 0.1 M KOH	50	2.4	Ref. 12
2D/1D Au/Pd	1.0 M ethanol + 1.0 M KOH	50	1.94	Ref. 13
Ni@Pd-Ni NAs	0.5M ethanol + 1.0 M KOH	50	0.96	Ref. 14
PdNN	1.0 M ethanol + 1.0 M KOH	50	2.38	Ref. 15

Table S5 Atomic ratio of Pd, Pt, and Au acquired from XPS analysis before and after the stability test of ethanol electrooxidation.

Catalysts	**Pd : Pt : Au before test**	**Pd : Pt : Au after test**	**$(Pd/Pt)_{Before}/(Pd/Pt)_{After}$**
$Pd_{14}Pt_5$	57.8 : 42.2 : 0 (100 : 73.0 : 0)	55.9 : 44.1 : 0 (100 : 78.9 : 0)	1.081
$Pd_{14}Pt_5Au_1$	56.6 : 37.3 : 6.1 (100 : 65.9 : 10.8)	54.8 : 38.4 : 6.8 (100 : 70.1 : 12.4)	1.063
$Pd_{14}Pt_5Au_2$	54.3 : 34.3 : 11.4 (100 : 63.2 : 21.0)	52.9 : 34.8 : 12.3 (100 : 65.8 : 23.3)	1.041
$Pd_{14}Pt_5Au_4$	47.0 : 29.0 : 24.0 (100 : 61.7 : 51.1)	45.8 : 29.3 : 24.9 (100 : 64.0 : 54.4)	1.036

Table S6 IR bands and their assignment appeared in the IR spectra of ethanol oxidation.

Species	Band center / cm^{-1}
CO_2	2343
CO_L on Pt	2014, 2029
CO_B on Pd	1952, 1902, 1923
CH_3COO^-	1552, 1415, 1346
CH_3CH_2OH	1046, 1085
HCO_3^-	1361

Supplementary References:

[1] S. G. Sun and Y. Lin, *Electrochim. Acta,* 1998, **44**, 1153-1162.

[2] N. Tian, Z. Y. Zhou, N. F. Yu, L. Y. Wang, S. G. Sun, *J. Am. Chem. Soc.,* 2010, **132**, 7580-7581.

[3] N. Tian, Z. Y. Zhou and S. G. Sun, *Chem. Commun.,* 2009, **12**, 1502-1504.

[4] W. K. Liang, Y. W. Wang, L. Zhao, W. Guo, D. Li, W. Qin, H. H. Wu, Y. H. Sun, L. Jiang, *Adv. Mater.,* 2021, **33**, 2100713.

[5] W. J. Huang, X. Y. Ma, H. Wang, R. F. Feng, J. G. Zhou, P. N. Duchesne, P. Zhang, F. J. Chen, N. Han, F. P. Zhao, J. H. Zhou, W. B. Cai, Y. G. Li, *Adv. Mater.,* 2017, **29**, 1703057.

[6] W. J. Huang, X. L. Kang, C. Xu, J. H. Zhou, J. Deng, Y. G. Li, S. Cheng, *Adv. Mater.,* 2018, **30**, 1706962.

[7] T. Wu, J. C. Fan, Q. X. Li, P. H. Shi, Q. J. Xu, Y. L. Min, *Adv. Energy Mater.,* 2018, **8**, 1701799.

[8] R. Kottayintavida and N. K. Gopalan, *Electrochim. Acta,* 2021, **384**, 138405.

[9] Y. Y. Liang, T. Ma, Y. Z. Xiong, L. Z. Qiu, H. Yu, F. Liang, *Nanoscale,* 2021, **13**, 9960-9970.

[10] M. L. Wang, D. Li, Y. Z. Tian, J. Zhao, Z. Z. Yue, X. X. Wang, X. F. Ma, J. J. Wang, T. J. Hu, J. F. Jia, H. S. Wu, *ACS Appl. Mater. Interfaces,* 2021, **13**, 53777-53786.

[11] T. Wu, Y. Ma, Z. B. Qu, J. C. Fan, Q. X. Li, P. H. Shi, Q. J. Xu, Y. L. Min, *ACS Appl. Mater. Interfaces,* 2019, **11**, 5136-5145.

[12] J. W. Hong, Y. Kim, D. H. Wi, S. Lee, S.-U.Lee, Y. W. Lee, S. I. Choi, S. W. Han, *Angew. Chem. Int. Ed.,* 2016, **55**, 2753-2758.

[13] C. H. Fang, T. Bi, Q. Ding, Z. Q. Cui, N. Yu, X. X. Xu, B. Y. Geng, *ACS Appl. Mater. Interfaces,* 2019, **11**, 20117-20124.

[14] F. Guo, Y. J. Li, B. A. Fan, Y. Liu, L. L. Lu, Y. Lei, *ACS Appl. Mater. Interfaces,* 2018, **10**, 4705-4714.

[15] H. Begum, M. S. Ahmed and S. Jeon, *ACS Appl. Mater. Interfaces,* 2017, **9**, 39303-39311.